OPEN ACCESS Freely available online

PLOS ONE

Waves of Calcium Depletion in the Sarcoplasmic Reticulum of Vascular Smooth Muscle Cells: An Inside View of Spatiotemporal Ca^{2+} Regulation

Mitra Esfandiarei*, Nicola Fameli, Yohan Y. H. Choi, Arash Y. Tehrani, Jeremy G. Hoskins, Cornelis van Breemen

Child & Family Research Institute, Department of Anaesthesiology, Pharmacology, and Therapeutics, University of British Columbia, Vancouver, British Columbia, Canada

Abstract

Agonist-stimulated smooth muscle Ca^{2+} waves regulate blood vessel tone and vasomotion. Previous studies employing cytoplasmic Ca^{2+} indicators revealed that these Ca^{2+} waves were stimulated by a combination of inositol 1,4,5-trisphosphate- and Ca^{2+}-induced Ca^{2+} release from the endo/sarcoplasmic reticulum. Herein, we present the first report of endothelin-1 stimulated waves of Ca^{2+} depletion from the sarcoplasmic reticulum of vascular smooth muscle cells using a calsequestrin-targeted Ca^{2+} indicator. Our findings confirm that these waves are due to regenerative Ca^{2+}-induced Ca^{2+} release by the receptors for inositol 1,4,5-trisphosphate. Our main new finding is a transient elevation in SR luminal Ca^{2+} concentration ($[Ca^{2+}]_{SR}$) both at the site of wave initiation, just before regenerative Ca^{2+} release commences, and at the advancing wave front, during propagation. This strongly suggests a role for $[Ca^{2+}]_{SR}$ in the activation of inositol 1,4,5-trisphosphate receptors during agonist-induced calcium waves. In addition, quantitative analysis of the gradual decrease in the velocity of the depletion wave, observed in the absence of external Ca^{2+}, indicates continuity of the lumen of the sarcoplasmic reticulum network. Finally, our observation that the depletion wave was arrested by the nuclear envelope may have implications for selective Ca^{2+} signalling.

Citation: Esfandiarei M, Fameli N, Choi YYH, Tehrani AY, Hoskins JG, et al. (2013) Waves of Calcium Depletion in the Sarcoplasmic Reticulum of Vascular Smooth Muscle Cells: An Inside View of Spatiotemporal Ca^{2+} Regulation. PLoS ONE 8(2): e55333. doi:10.1371/journal.pone.0055333

Editor: Ladzlo Csernoch, University of Debrecen, Hungary

Received October 30, 2012; **Accepted** December 20, 2012; **Published** February 7, 2013

Copyright: © 2013 Esfandiarei et al. This is an open-access article distributed under the terms of the Creative Commons Attribution License, which permits unrestricted use, distribution, and reproduction in any medium, provided the original author and source are credited.

Funding: This study was supported by the operating grant (FRN#84309) from the Canadian Institutes of Health Research. The funders had no role in study design, data collection and analysis, decision to publish, or preparation of the manuscript.

Competing Interests: The authors have declared that no competing interests exist.

* E-mail: mesfandiarei@gmail.com

Introduction

In vascular smooth muscle cells (VSMCs), fluctuations in cytoplasmic Ca^{2+} concentration ($[Ca^{2+}]_i$) selectively control multiple functions, including contraction-relaxation, energy metabolism, proliferation, migration and apoptosis, in health and disease [1,2,3,4,5]. It is generally accepted that functional selectivity of Ca^{2+} signals is encoded in their spatial and temporal characteristics [6,7,8]. In this context, we support the view that the ubiquitous asynchronous Ca^{2+} waves in VSM are optimally suited to couple agonist-mediated stimulation to vasoconstriction in healthy blood vessels, while avoiding recruitment of stress related functions [2,3,9], [10]. Neylon and coworkers were the first to report that receptor stimulation of cultured human VSM did not simply elevate $[Ca^{2+}]_i$ to induce activation, but in fact caused a wave of elevated $[Ca^{2+}]_i$ to travel across the cell from an initiation site [11]. They further proposed a mechanism involving stimulation of inositol 1,4,5-trisphosphate receptors (IP_3R) and Ca^{2+} induced Ca^{2+} release (CICR) [11]. In 1994, Iino *et al.* made the next advance by recording $[Ca^{2+}]_i$ in the intact rat tail artery smooth muscle [4]. Iino had earlier discovered that IP_3Rs were sensitive to Ca^{2+}, such that IP_3 required Ca^{2+} as a co-activator, and that the elevation of $[IP_3]_i$ facilitates CICR at IP_3Rs [12]. Sympathetic nerve stimulation initiated asynchronous repetitive waves of $[Ca^{2+}]_i$ elevation, traveling in both directions along the length of the spirally arranged smooth muscle fibres. The unexpected aspect of this discovery was that the tonic increases in both the bulk smooth muscle $[Ca^{2+}]_i$ and force were based on wave-like $[Ca^{2+}]_i$ oscillations in individual VSMCs. Because of the asynchronous nature of these cellular Ca^{2+} waves, summation over thousands of cells in the vascular media results in maintained average $[Ca^{2+}]_i$ elevation and vascular tone. Nevertheless, the repetitive Ca^{2+} waves would still confer the advantage of added informational content due to frequency encoding and prevention of potential harm due to prolonged elevated $[Ca^{2+}]_i$.

Although a great deal of valuable information has subsequently accumulated on the mechanism of Ca^{2+} waves, previous studies were limited, to some degree, by the fact that they reported changes in cytoplasmic Ca^{2+}, which represent the result of Ca^{2+} release from the sarcoplasmic reticulum (SR) rather than the process itself. In this study, in order to obtain more direct insight into regenerative Ca^{2+} release in VSMCs, we have used a specific Ca^{2+} indicator targeted to calsequestrin in the SR lumen that we refer to as D1SR. The VSMCs used in this study constituted a primary culture, which remained highly contractile during the study. Here, we report a wave of Ca^{2+} depletion from the SR itself, which in this case is activated by applying the vascular autocoid endothelin-1 (ET-1). The observed agonist-induced SR Ca^{2+}

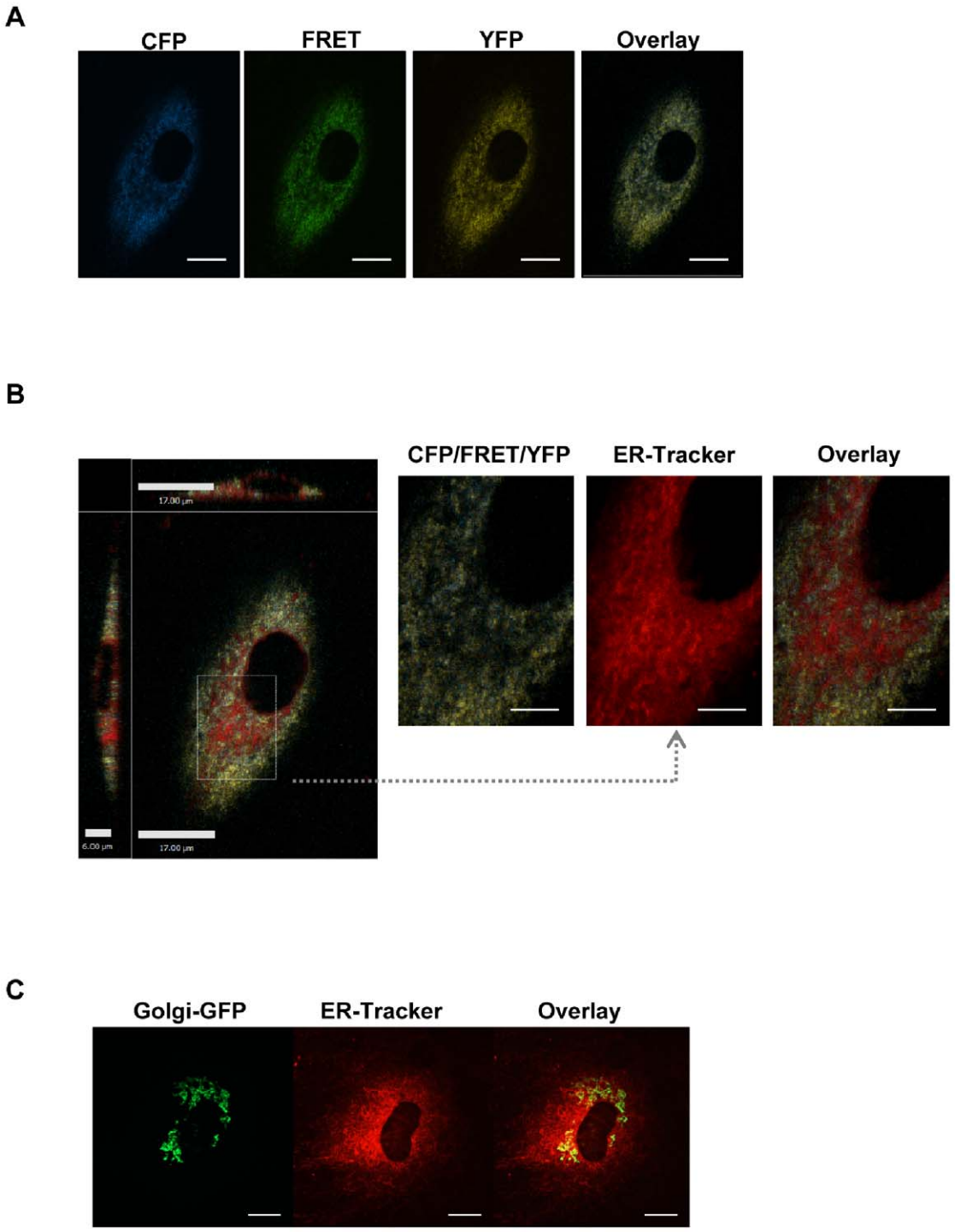

Figure 1. Distribution of D1SR Ca^{2+} indicator in rat aortic SMCs. A) Fluorescence images of D1SR indicator distribution using CFP (440/488 nm), FRET (440/535 nm), and YFP (514/535 nm) band-pass filters (scale bars, 10 μm). **B)** 2-D projection of a merged fluorescence image of D1SR using CFP (440 nm excitation/488 nm emission), FRET (440 nm excitation/535 nm emission), and YFP (514 nm excitation/535 nm emission) band-pass filters, and ER-Tracker™ Red (587 nm excitation/615 nm emission) are shown. The majority of area shows overlay of D1SR and SR lumen tracker. The zoomed-in images highlight areas of SR lumen negative for D1SR signal, but positive for ER-Tracker. In all experiments, such areas were excluded from data analyses (scale bars, 10 μm unless indicated otherwise). **C)** SMCs are loaded with Golgi-GFP CellLight® solution for 16 hours at 37°C prior to loading with ER-Tracker™ Red dye for 15 minutes. Fluorescence images of ER-Tracker™ Red (587 nm excitation/615 nm emission) and Golgi-GFP (488 nm excitation/520 nm emission) are shown (scale bars, 10 μm).
doi:10.1371/journal.pone.0055333.g001

depletion wave provides valuable new information about the role of SR luminal Ca^{2+} concentration ($[Ca^{2+}]_{SR}$) in the initiation and propagation of Ca^{2+} waves, which was not attainable by recording fluctuations in $[Ca^{2+}]_i$.

Materials and Methods

Buffers & Reagents

HEPES-PSS containing (in mmol·L^{-1}) NaCl 140, glucose 10, KCl 5, HEPES 5, $CaCl_2$ 1.5 and $MgCl_2$ 1 (pH 7.4) was used for all calcium measurements and confocal microscopy. The nominal zero-Ca^{2+} PSS was prepared in the same way as normal PSS without the addition of calcium. Endothelin-1 (ET-1) was obtained from Sigma-Aldrich (ON, Canada). Thapsigargin (Tg), a cell permeable inhibitor of sarcoplasmic reticular Ca^{2+}-ATPase (SERCA), and xestospongin C (Xes-C), a potent membrane-permeable blocker of IP_3-mediated Ca^{2+} release, were purchased from EMD Chemicals (NJ, USA). Sodium orthovanadate, an inhibitor of secretory pathway Ca^{2+} ATPase (SPCA) pumps, was purchased from Sigma-Aldrich. Stock solutions of ET-1 and Tg were prepared in dimethyl sulfoxide (DMSO). For all experiments, vehicle-treated (0 μM) groups were incubated with equal volume of DMSO, respectively (the maximum volume of solvents used with the highest concentration of drugs). Further dilutions of reagents were made in zero-Ca^{2+} PSS buffer. The calcium dye Fluo-4 AM, ER-Tracker, Mito-Tracker Green FM, BODIPY® TR-X thapsigargin, and CellLight™ Golgi-GFP BacMam 2.0 were all purchased from Invitrogen (ON, Canada).

Cell Culture

Rat aortic SMCs were originated from the laboratories of Drs. Urs Ruegg and Nicolas Demaurex (University of Geneva, Geneva, Switzerland), and prepared from aorta of male Wistar Kyoto rats (200–300 g) as previously described [13]. Cells between passage 9 to 13 were cultured in Matrigel-coated (BD Sciences; ON, Canada) 35 mm glass bottom culture dishes (MatTek Co., MA, USA), and grown in Dulbecco's modified Eagle's medium supplemented with 10% heat-inactivated newborn calf serum, Penicillin G (100 μg.mL^{-1}), and streptomycin (100 μg.mL^{-1}) (Invitrogen, ON, Canada) at 37°C, in a humidified incubator in 5% CO_2. See following sections for a detailed description of the transfection protocol and buffer/reagents used in the study.

Transient Transfection with D1SR Constructs

D1SR indicator, a modified variant of the D1ER cameleon [14,15,16], is kindly provided by Dr. Wayne Chen (University of Alberta, Canada). In the D1SR indicator, the original calreticulin signal sequence in D1ER has been replaced by the mutant calsequestrin sequence with a reduced binding ability to calcium (to eliminate the competition with endogenous calsequestrin in binding to calcium ion within SR). The D1SR construct consists of a truncated enhanced CFP and YFP that are joined by a linker containing modified calmodulin (CaM) and M13 (the 26-residue CaM-binding peptide of myosin light-chain kinase) sequences. The CaM-M13 modifications prevent M13 from binding endogenous calmodulin. SR retention is achieved by calcequestrin sequences on the 5′ end of CFP. Following binding to Ca^{2+}, conformational changes in the CaM-M13 domain increase the fluorescence resonance energy transfer (FRET) between the flanking CFP and YFP yielding a Ca^{2+} response. SMCs were transfected with adenoviral D1SR constructs at a multiplicity of infection of 100 (MOI = 100). Following overnight incubation at 37°C, cells were replenished with fresh medium. Fluorescence microscopy was used to assess transfection efficiency and cellular

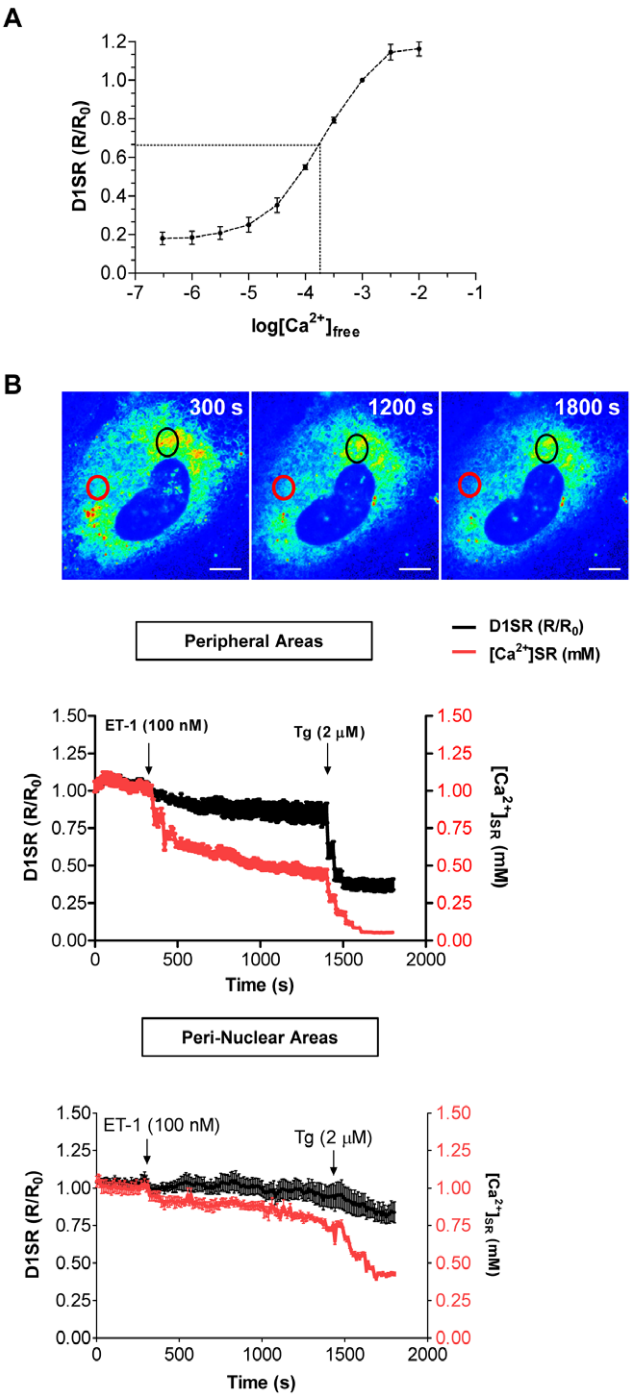

Figure 2. Calibration of D1SR *in situ* and effects of endothelin-1 and thapsigargin on SR Ca^{2+} signal. A) D1SR fluorescent ratio was calibrated *in situ* in semi-permeabilized SMCs (n = 12 cells from four independent culture plates, mean ± SEM) in intracellular solutions with 0.001 to 10 mM of free Ca^{2+}, and fitted to an exponential equation. **B)** Selected snapshots from a time-lapse movie (10 s intervals) of rat SMCs transfected with D1SR indicator (scale bars, 5 μm), and averaged R/R_0 and corresponding $[Ca^{2+}]_{SR}$ values in peripheral (red circle) and peri-nuclear (black circle) areas in response to ET-1 (100 mM) and Tg (2 μM) treatments in the presence of extracellular Ca^{2+}. As illustrated, ET-1 causes a slight change in R/R_0 values in the peri-nuclear area (ROIs = 20, n = 6 independent experiments, mean ± SEM, $P<0.005$).
doi:10.1371/journal.pone.0055333.g002

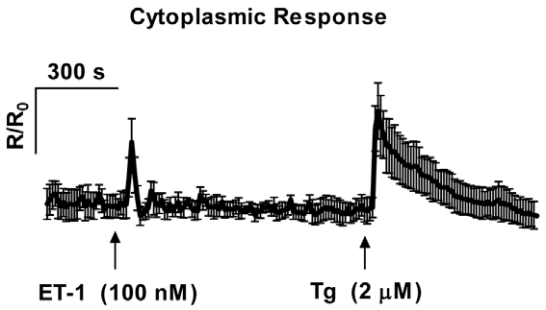

Figure 3. Effects of endothelin-1 and thapsigargin on cytoplasmic Ca^{2+} signal. Average trace of cytoplasmic Ca^{2+} signals recorded (10 s intervals) in rat SMCs loaded with Ca^{2+} indicator Fluo-4 AM. ET-1 (100 nM) initially causes a spike in $[Ca^{2+}]_i$, and subsequent inhibition of SERCA with 2 μM Tg elicits another large $[Ca^{2+}]_i$ transient due to depletion of SR luminal Ca^{2+} (ROI = 15, n = 4 independent experiments, mean ± SEM, $P<0.005$).
doi:10.1371/journal.pone.0055333.g003

morphology at 48 h post transfection. For all experiments, a transfection efficiency of 80–90% was achieved.

SR Luminal Ca^{2+} Measurement

Ratiometric FRET images were acquired with a 63× oil-immersion objective (Leica DM16000 inverted microscope) and a cooled Hamamatsu 9100-02 electron multiplier CCD camera. Cells were excited at 440 nm, and 513 nm; and imaged using 488 nm/535 nm (for donor and FRET channels) and 535 nm (for acceptor channel) band-pass filters (three images/time point). The acceptor channel was simultaneously recorded to monitor photobleaching. We set the intensity of light at 15% transmitted light, and excitation exposure times at 150 ms with 10 s intervals.

Cytoplasmic Ca2+ Measurement

During *in vitro* measurement of cytoplasmic Ca^{2+} signals, all parameters (laser intensity, gain, etc.) were maintained constant during the experiment. The cell culture was illuminated using an Argon-Krypton laser (488 nm) and a high-gain photomultiplier tube collected the emission (505–550 nm). The customized Hamamatsu 9100-02 electron multiplier CCD camera delivers 1000×1000 pixels, imaged to Shannon-Nyquist specifications for the 63× objectives, providing a larger field of view. The representative fluorescence traces shown reflect the averaged fluorescence signals from 15 regions of interest (ROIs) in each cell. The measured changes in Fluo-4 AM fluorescence level are proportional to the relative changes in cytoplasmic Ca^{2+} ($[Ca^{2+}]_i$). The confocal images were analyzed off-line with the Improvision Volocity software (Perkin-Elmer). Fluorescence traces were extracted from the movies and were normalized to initial fluorescence values.

Image Analysis

All data used for Ca^{2+} traces were analyzed by Improvision Volocity software, using built-in regions-of-interest (ROI) function to select the areas of interest that is at least 30 pixels long in length and width. For traces involving specific sites, shape and size of ROI were adjusted to avoid artifacts and saturated areas. For distance and velocity analysis, one ROI was selected per frame (time point) based on the movement of the Ca^{2+} wave. The resulting data were formatted on Microsoft Excel 2007, and analyzed by GraphPad Prism 5.0. Pseudo-colour visualization was performed by ImageJ, using customized lookup tables to assign colour for each pixel intensity values. Line scan was performed first by analyzing pixel intensity of a series of small ROIs (1–3 pixels in length per ROI) along a line using a customized Python script to output change in intensity over time along the line. The script was confirmed to output same values when analyzing same ROI on Volocity. The resulting values were then graphed using Gnuplot 4.4 with custom lookup table.

Statistical Analysis

Data are presented as means ± SEM of at least four independent experiments. Significance was determined using Student's *t*-test with two-tailed distribution using GraphPad Prism 5 ($P \leq 0.05$ was considered as statistically significant).

Results

Distribution of D1SR Ca^{2+} Indicator in Rat Aortic SMCs

To monitor fluctuations in $[Ca^{2+}]_{SR}$, we transfected rat aortic SMCs with an adenoviral vector expressing the specific FRET-based SR Ca^{2+} indicator, D1SR. Figure 1A shows the individual and merged fluorescence images of three recorded channels (CFP: 440 nm/488 nm; FRET: 440 nm/535 nm; YFP: 513 nm/535 nm) for D1SR indicator in cultured VSMCs (see Movie S1). We also compared the distribution of D1SR with that of ER-Tracker, commonly used for localization of either ER or SR. As expected, D1SR co-localizes with ER-Tracker except for a region close to the nucleus that is negative for D1SR fluorescence, but positive for ER-Tracker (Fig. 1B). Specific staining with Golgi-Tracker indicated that the Golgi apparatus is typically located in this region (Fig. 1C).

D1SR Calibration *in situ*

The D1SR indicator was calibrated *in situ* in semi-permeablilized rat aortic SMCs in intracellular HEPES solution (135 mM KCl, 10 mM NaCl, 1 mM $MgCl^2$, 20 mM HEPES, 20 mM sucrose, 0.01 mM digitonin, 0.01 mM ionomycin, 0.005 mM CCCP, PH 7.2) with 5 mM HEDTA as described before [16]. The intracellular solution was blended with the stock solution of 100 mM $CaCl_2$ to prepare buffers with free Ca^{2+} concentrations ($[Ca^{2+}]_{free}$) ranging from 1 μM to 10 mM (Max Chelator v2.40, C. Patton, Standford University, USA, maxchelator.stanford.edu). D1SR fluorescent ratio (R/R_0) was plotted against $[Ca^{2+}]_{free}$ in 12 cells from four independent cultures and an exponential fit was applied to the data to determine the apparent dissociation constant K_d (197±47 μM) and the Hill slope ($n = 0.87 \pm 0.19$) (Fig. 2A). $[Ca^{2+}]_{SR}$ was calculated by calibrating normalized D1SR ratio against the standard calibration curve as described previously [16]. To calculate $[Ca^{2+}]_{SR}$, normalized ratio values were fitted to:

$$\mathrm{R/R0} = R\mathrm{min/R0} \times \frac{[(R\mathrm{max/R0}) - (R\mathrm{min/R0})]}{1 + 10^{(\mathrm{LogK'}d - \mathrm{Log[Ca2+]SR})n}}$$

where R_{min} and R_{max} were obtained by measuring signal intensity in cells perfused with intracellular HEPES solution containing 5 mM HEDTA (Calcium free buffer) and 10 mM free calcium (15 mM CaHEDTA), respectively.

Effects of Endothelin-1 and Thapsigargin on SR and Cytoplasmic Ca^{2+} Signals

The traces in Figure 2B illustrate the effects of receptor activation with ET-1 (100 nM) and SERCA inhibition with 2 μM thapsigargin (Tg) on $[Ca^{2+}]_{SR}$ in the peripheral (marked with red circle) and peri-nuclear (marked with black circle) areas of SMCs.

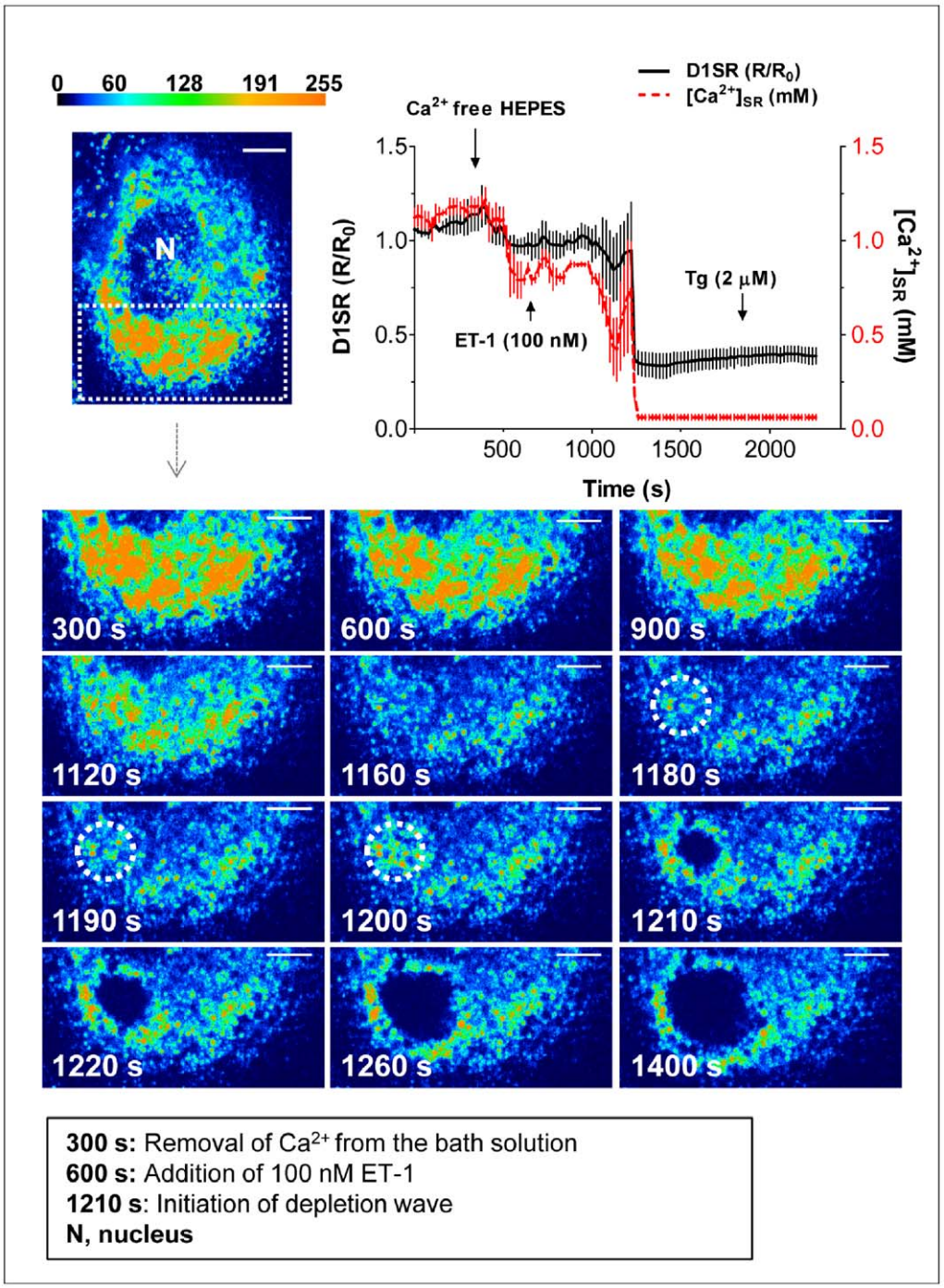

Figure 4. Progression of ET-1-induced regenerative Ca^{2+} depletion wave in the absence of extracellular Ca^{2+}. Average trace for R/R_0 values in SMCs treated with ET-1 (100 nM) and Tg (2 uM) in the absence of extracellular Ca^{2+}. ET-1 induces a delayed bi-phasic drop in $[Ca^{2+}]_{SR}$, a small initial transient phase, followed by a large precipitous drop in $[Ca^{2+}]_{SR}$ (n = 6 independent experiments, mean ± SEM, $P<0.005$). Representative snapshots (FRET channel) of time-lapse movie (10 s intervals) illustrates an ET-1-induced regenerative Ca^{2+} depletion wave over time in a SMC (scale bars, 4.3 μm). At 300 s, the bathing solution is replaced by nominal Ca^{2+} free HEPES. At 600 s, ET-1 (100 nM) is added, which elicits a delayed decrease in luminal Ca^{2+} around 1160 s post-treatment. Immediately prior to the initiation of the depletion wave, a rapid transient increase in Ca^{2+} is observed at the point of origin (1200 s panel, circled area), followed by a significant drop due to wave development.
doi:10.1371/journal.pone.0055333.g004

In the cell periphery, ET-1 causes a drop in $[Ca^{2+}]_{SR}$ (from 1.08±0.12 mM to 450±50 μM), and subsequent SERCA inhibition results in an additional decline (to 55±11 μM). In the peri-nuclear areas, however, the ET-stimulated changes in $[Ca^{2+}]_{SR}$ are moderate (from 1.05±0.07 mM to 700±50 μM). Although a clear loss of $[Ca^{2+}]_{SR}$ is evident following Tg application, a considerable amount of D1SR signal remains in the peri-nuclear areas (427±23 μM), indicating the presence of organelles containing calsequestrin and Ca^{2+} that are not sensitive to SERCA blockade. A plausible explanation for this residual

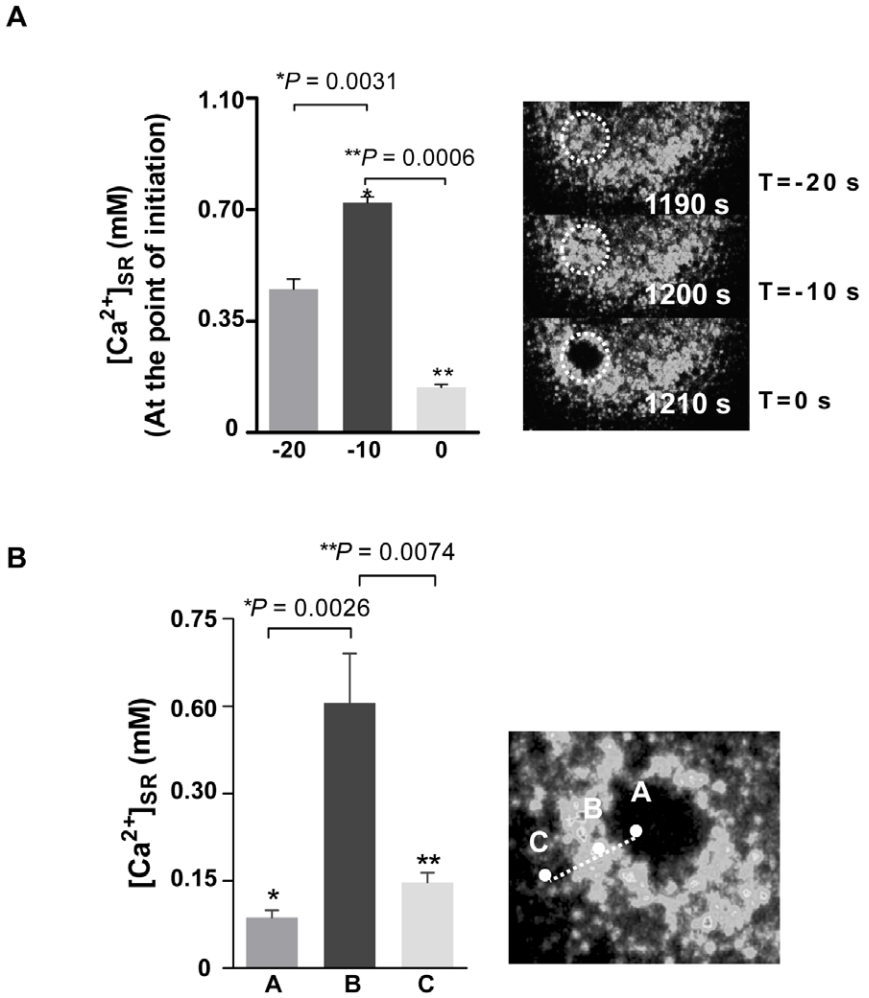

Figure 5. Characteristics of the ET-1-induced Ca^{2+} depletion waves. A) Average changes in Ca^{2+} signal intensity at the points of initiation. T = 0, T = −10 s, and T = −20 s refer to the time when the depletion wave first appears and 10 and 20 s prior to wave initiation, respectively. The Ca^{2+} signal significantly increases at T = −10 s, and drops to a low level as the waves initiate at T = 0 s (n = 5 cells from five independent experiments, mean ± SEM, *P = 0.0031, **P = 0.0006). **B)** R/R_0 values in three regions of the depletion wave (A: already depleted area; B: area that has taken up released Ca^{2+}; C: area not yet affected by the wave B). At any given time point, the signal intensity at the rim (point B) is higher than both the already depleted area (point A) and the adjacent SR locus ahead of the wave (point C) (ROI = 4, n = 5 independent experiments, mean ± SEM, *P = 0.0026, **P = 0.0074).
doi:10.1371/journal.pone.0055333.g005

$[Ca^{2+}]_{SR}$ is that in these cells the SR is contiguous with membranous organelles or endosomes, which accumulate Ca^{2+} via the Tg-insensitive "secretory pathway Ca^{2+} ATPase" (SPCA). An alternative explanation is provided by a recent report from Ledeen's group [17], which showed that NCX located in the inner membrane of the nuclear envelope is able to take up Ca^{2+} after SERCA blockade. Furthermore, since the nuclear envelope and the SR are confluent, this Ca^{2+}, taken up by the NCX is capable of diffusing into the peri-nuclear SR.

In order to compare the changes in $[Ca^{2+}]_{SR}$ with fluctuations in $[Ca^{2+}]_i$, we used the cytoplasmic Ca^{2+} indicator fluo-4 AM in the same VSMC preparation (Fig. 3). In these cells, ET-1 (100 nM) appears to be a weak agonist eliciting only a transient increase in $[Ca^{2+}]_i$ as opposed to uridine-5′-triphosphate (UTP), which stimulates a large maintained increase in $[Ca^{2+}]_i$. Subsequent inhibition of SERCA with Tg (2 μM) elicits another large $[Ca^{2+}]_i$ transient due to depletion of SR luminal Ca^{2+}. Therefore, at least in the case of ET-1, it is clear that the luminal SR Ca^{2+} indicator shows dynamics, which are different from those observed with the cytoplasmic Ca^{2+} sensitive dye, fluo-4 AM.

ET-1-induced Regenerative SR Ca^{2+} Depletion Waves in the Absence of Extracellular Ca^{2+}

In order to distinguish the effects of ET-1 on luminal SR Ca^{2+} from those related to ET-1 stimulated Ca^{2+} entry from the extracellular space, we removed Ca^{2+} from the bathing solution, but without adding a chelator. Under these conditions, which inhibit SR Ca^{2+} refilling [18], ET-1 caused a large and delayed drop in $[Ca^{2+}]_{SR}$ (Fig. 4). The difference between ET-induced responses in the presence and absence of external Ca^{2+} is not surprising, because in the presence of external Ca^{2+}, there is rapid Ca^{2+} cycling between the SR lumen and extracellular space [19], which appears to protect the SR from excessive Ca^{2+} depletion. In contrast, in nominally Ca^{2+} free condition, which inhibits SR refilling, ET-1 causes a much larger drop in $[Ca^{2+}]_{SR}$.

In about 80% of the cells, application of ET-1 after removal of external Ca^{2+} revealed a novel phenomenon that we refer to as the

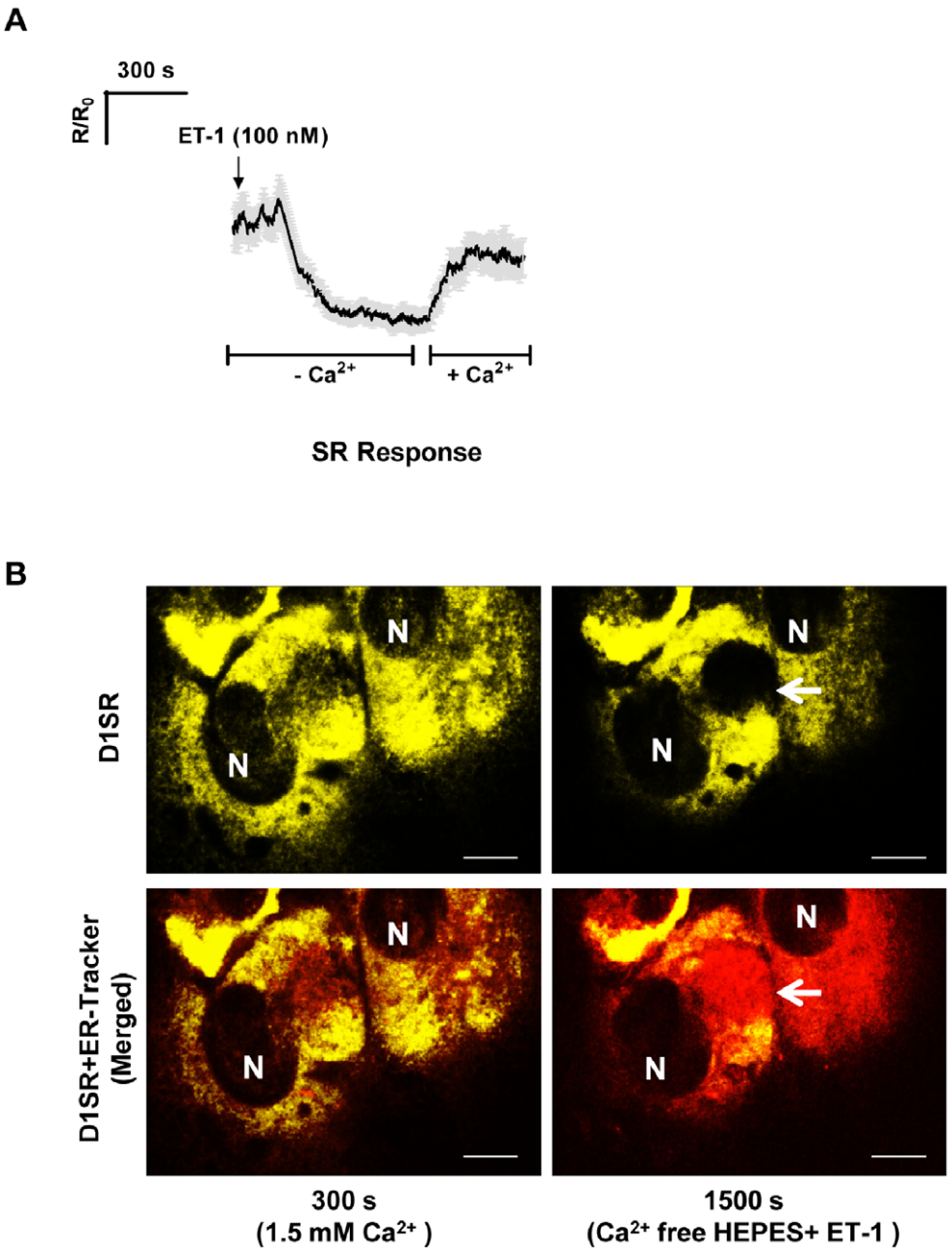

Figure 6. Refilling of SR Ca^{2+} and maintenance of SR structure following the depletion wave. A) The SR is refilled by subsequent re-perfusion of the cell culture with normal (1.5 mM) Ca^{2+} solution following depletion wave progression, confirming the reversibility of Ca^{2+} depletion wave. **B)** Live snapshots of overlay of D1SR and ER-Tracker signals in cultured SMCs showing that the SR luminal structure remains intact during and after the progression of ET-induced Ca^{2+} deletion wave (marked by white arrows) and in the absence of extracellular Ca^{2+}. (scale bars, 15 μm).
doi:10.1371/journal.pone.0055333.g006

"SR Ca^{2+} depletion wave" (Fig. 4 and Movie S2). At 300 s, Ca^{2+} is removed from the bathing solution, and at 600 s, ET-1 (100 nM) is added. In the presence of ET-1, focal fluctuations in $[Ca^{2+}]_{SR}$ can be observed, and just before the onset of the Ca^{2+} depletion wave, $[Ca^{2+}]_{SR}$ is elevated at the site of wave initiation (Fig. 4, panel 1200 s). The SR depletion waves routinely originated close to the peri-nuclear region, rather than in the cell periphery.

Measurements of changes in the R/R_0 values at the point of wave initiation, confirmed a transient increase in $[Ca^{2+}]_{SR}$ to 700±100 μM immediately prior to wave initiation (Fig. 5A). Subsequently a depletion of $[Ca^{2+}]_{SR}$ occurs at the site of initiation (from 700±100 μM to 60±20 μM), from which a wave of Ca^{2+} depletion radiates out into the surrounding SR network (Fig. 4, panels 1210–1400 s). In the absence of external Ca^{2+} the extent of ET-1-induced $[Ca^{2+}]_{SR}$ depletion is similar to that induced by Tg. The depletion wave progresses in a roughly circular fashion and is always surrounded by a rim of elevated $[Ca^{2+}]_{SR}$. It thus appears that some of the Ca^{2+} released at the wave front is taken up by an adjacent, but not-yet-activated SR locus. Figure 5B shows that at any given time point of wave expansion, there are significant differences in $[Ca^{2+}]_{SR}$ between the depleted SR region (marked as A), the transiently refilled neighbouring SR locus (marked as B),

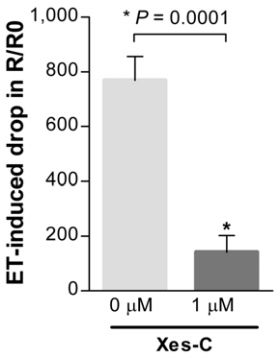

Figure 7. Ca^{2+} depletion waves propagate via IP_3Rs. Inhibition of IP_3Rs with Xes-C (1 μM) blocks ET-induced depletion waves as compared to vehicle-control groups. For Xes-C treated groups, cells were perfused with nominal Ca^{2+} free buffer containing 1 μM Xes-C starting 5 min prior to addition of ET-1 (n = 5 cells from five independent experiments, mean ± SEM, *$P = 0.0001$).
doi:10.1371/journal.pone.0055333.g007

and the next SR locus further ahead of the depletion wave (marked as C). After passage of the ET-induced Ca^{2+} depletion wave, the SR was capable of refilling upon subsequent re-perfusion with normal (1.5 mM) Ca^{2+} solution, confirming the reversibility of the observed SR depletion wave (Fig. 6A). Furthermore, the depletion waves recorded herein did not cause any long-lasting structural changes in SMCs, and the SR structure remained intact during the experiment (Fig. 6B).

Ca^{2+} Depletion Waves in SMCs Propagate via IP_3 Receptors

A plausible explanation for the initiation of SR Ca^{2+} depletion waves is that after the IP_3 concentration builds up to a critical level and the cytoplasmic and SR Ca^{2+} concentrations at the initiation site reach a certain threshold values, the IP_3Rs on the SR membrane open in a regenerative fashion; the wave is then propagated by CICR at IP_3Rs. To test this hypothesis, we blocked the IP_3Rs with a specific inhibitor xestospongin C (Xes-C) prior to the application of ET-1 (Fig. 7). Addition of Xes-C (1 μM) completely blocked ET-induced depletion waves, confirming that as for other VSM Ca^{2+} waves [8,18,20], the underlying mechanism is indeed mediated by CICR at IP_3R. This notion was further corroborated by the observation that our cultured SMCs failed to respond to caffeine (data not shown), confirming the lack of functional RyRs in these cells, which is in agreement with a previous report by Vallot et al [21].

Dynamics of the Ca^{2+} Depletion Waves in the SR Lumen

Another instructive way of analyzing the $[Ca^{2+}]_{SR}$ depletion wave is to identify a line intersecting the site of wave initiation and recording the changes in R/R_0 values along this line *vs.* time (line scan). The resulting "heat map" illustrates that initially the area of $[Ca^{2+}]_{SR}$ depletion expands rapidly, but as time proceeds, it asymptotically approaches a final limit (Fig. 8A). Analysis of a number of such heat maps yields the average distance *vs.* time, as well as the velocity *vs.* time curves (Fig. 8B). Extrapolation of the velocity curve to the time of wave initiation (0 s), shows that the SR Ca^{2+} depletion wave has an initial velocity of about 0.7 μm/s, which falls below the range (2–30 μm/s) reported previously for intact smooth muscle Ca^{2+} waves in the presence of extracellular Ca^{2+} [22]. This could be explained by the fact that in our cultured VSMCs, ET-1 is a weak agonist, and a number of studies have shown that both the velocity and frequency of smooth muscle Ca^{2+} waves increase with the level of activation and the concentration of IP_3 [8,23]. The profound decrease in velocity over time is likely related to the decline of the $[Ca^{2+}]_{SR}$ at the rim as the wave progresses (Fig. 8C).

Quantitative Model for Propagation of Ca^{2+} Depletion Waves

The observed transient increase in $[Ca^{2+}]_{SR}$ at both the origin and the rim of the depletion wave (Fig. 5A and 5B) suggests an important role for local $[Ca^{2+}]_{SR}$ elevation during initiation and propagation of regenerative IP_3R-mediated Ca^{2+} release. Since in cytoplasmic Ca^{2+} oscillations, the latency period is related to the inter-spike interval [24], which is, in turn, regulated by the SR Ca^{2+} content [24], the VSMCs activity may well be controlled by focal fluctuations in $[Ca^{2+}]_{SR}$. In line with previous reports [25,26], we propose that these fluctuations are generated in part by a differential distribution of SR luminal Ca^{2+} sinks (clusters of IP_3Rs), and Ca^{2+} sources (SERCA) (Fig. 9A). Stochastic opening of individual IP_3Rs (which yield cytoplasmic Ca^{2+} blips) [25,26] would add variability to focal $[Ca^{2+}]_{SR}$. Whenever an increase in local $[Ca^{2+}]_{SR}$ exceeds the threshold for regenerative opening of an IP_3R cluster, sufficient Ca^{2+} would be released to initiate a regenerative Ca^{2+} wave.

Generation of a wave according to this mechanism, and possessing the features of deceleration and decreasing intensity at the progressing rim as we observe, implies a continuity of the SR lumen. Since under control conditions the non-activated SR remains loaded with Ca^{2+} because of continual activity of SERCA, the observed decline in $[Ca^{2+}]_{SR}$ at the rim of the depletion wave (Fig. 8C) is a strong indication that a re-equilibration of the SR Ca^{2+} content is taking place within the SR lumen. Only in this manner, when removal of extracellular Ca^{2+} blocks SR refilling, then opening of IP_3Rs at the wave front would partially deplete the SR located just ahead of the wave.

To analyze this proposed mechanism, we developed a preliminary and simplified two-dimensional quantitative model for the propagation of the observed depletion waves, which is based on previous observations and suggested models arguing for 1) a continuous SR lumen in regards to Ca^{2+} transport, 2) the appearance of functionally segregated compartments in the SR of SMCs, and 3) the existence of a luminal Ca^{2+} binding site of the IP_3R [27,28,29]. The essential steps of this model are presented in Figure 9B, and the generated trace for the velocity of the depletion wave is presented in Figure 9C.

Using the symbols and data in Table 1, our model assumes that, before any Ca^{2+} depletion wave (CDW) event, the $[Ca^{2+}]_{SR}$ is at a normal resting level (C_{SR}) and that it needs to reach a critical level (C^*_{SR}) for release. Then, for example, following the depletion of a given SR compartment, for a nearest neighbouring compartment to release, its $[Ca^{2+}]_{SR}$ needs to change by $C^*_{SR} - C_{SR} = 200$ μM, which translates to about 1500 Ca^{2+}. For the sake of order-of-magnitude calculations, let us say that SERCA pumps operating at 300 s^{-1} would take a time interval $\Delta t_1 = 5$ s to cause a 200 μM $[Ca^{2+}]_{SR}$ change. We calculate the depletion wave velocity, v_{CDW}, as the inter-IP_3R-cluster distance, d, divided by the time, Δt, taken to raise the $[Ca^{2+}]_{SR}$ in the new compartment from normal to critical: $v_{CDW} = d/\Delta t$. For the sake of completeness, the wave velocity should also include a component for the Ca^{2+} diffusion time from cluster to cluster. This component is however of the order of milliseconds and therefore negligible when compared to SR compartment refill times.

In this manner, for one depletion wave "step" in our model (from compartment 0 to 1 in Figure 9B), $v_{CDW,1} = d/\Delta t_1 = 0.1$ μm/

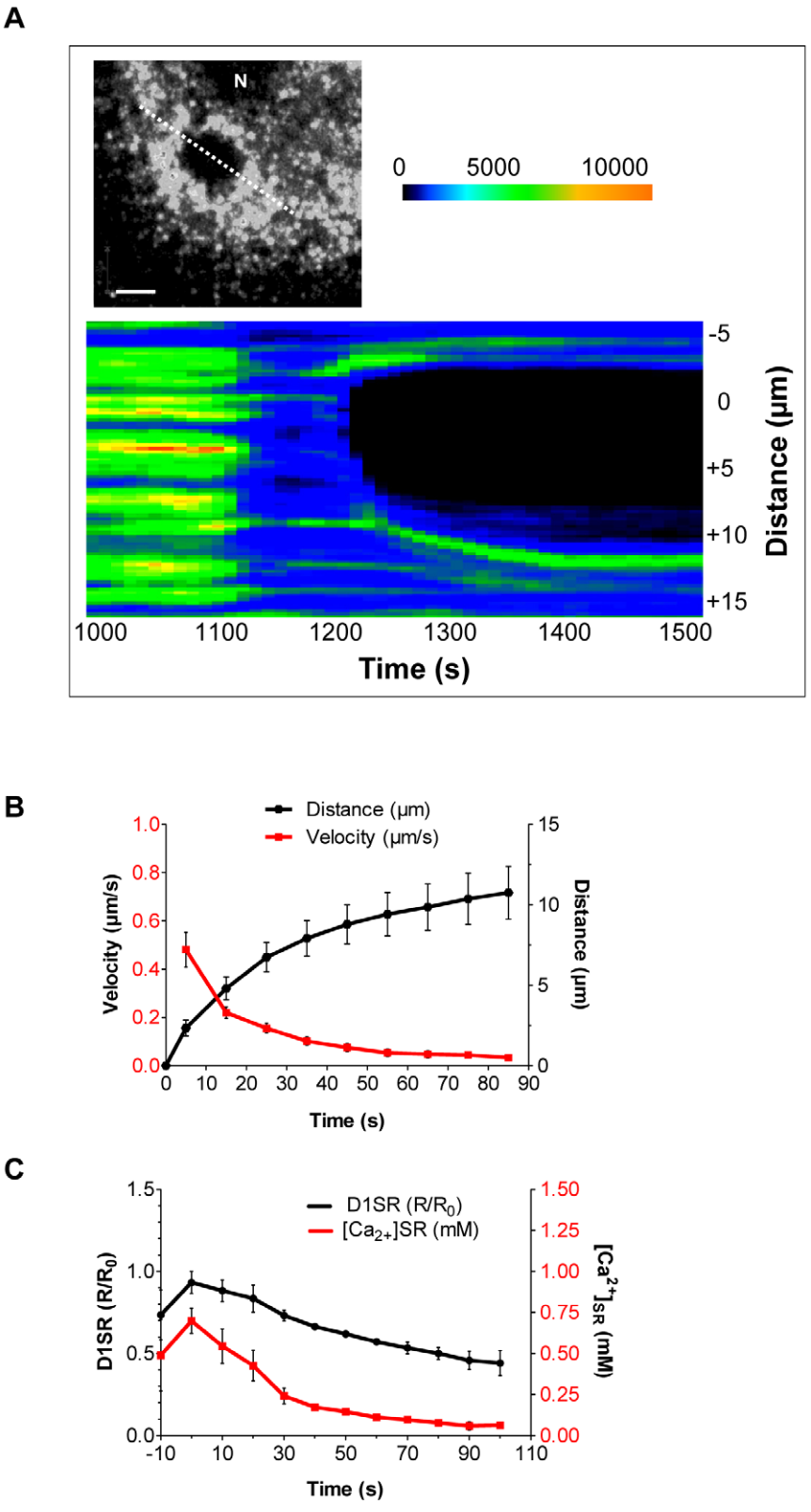

Figure 8. Dynamics of the Ca^{2+} depletion waves. A) Heat map generated from the time-lapse fluorescence microscopy movie (10 s intervals) of rat SMCs treated with ET-1 (100 nM) in nominally free extracellular Ca^{2+}, showing that the SR depletion wave expands in a near circular fashion in both directions of the scan line (dotted white line). **B)** Average travel distance and velocity of ET-1-induced depletion wave *vs.* time. As the distance from the point of origin increases, the wave velocity decreases asymptotically to zero. **C)** Average values for R/R_0 and $[Ca^{2+}]_{SR}$ at the rim of the depletion wave also decreases as the wave expands over time (ROI = 5, n = 5 independent experiments, mean ± SEM, $P<0.005$).
doi:10.1371/journal.pone.0055333.g008

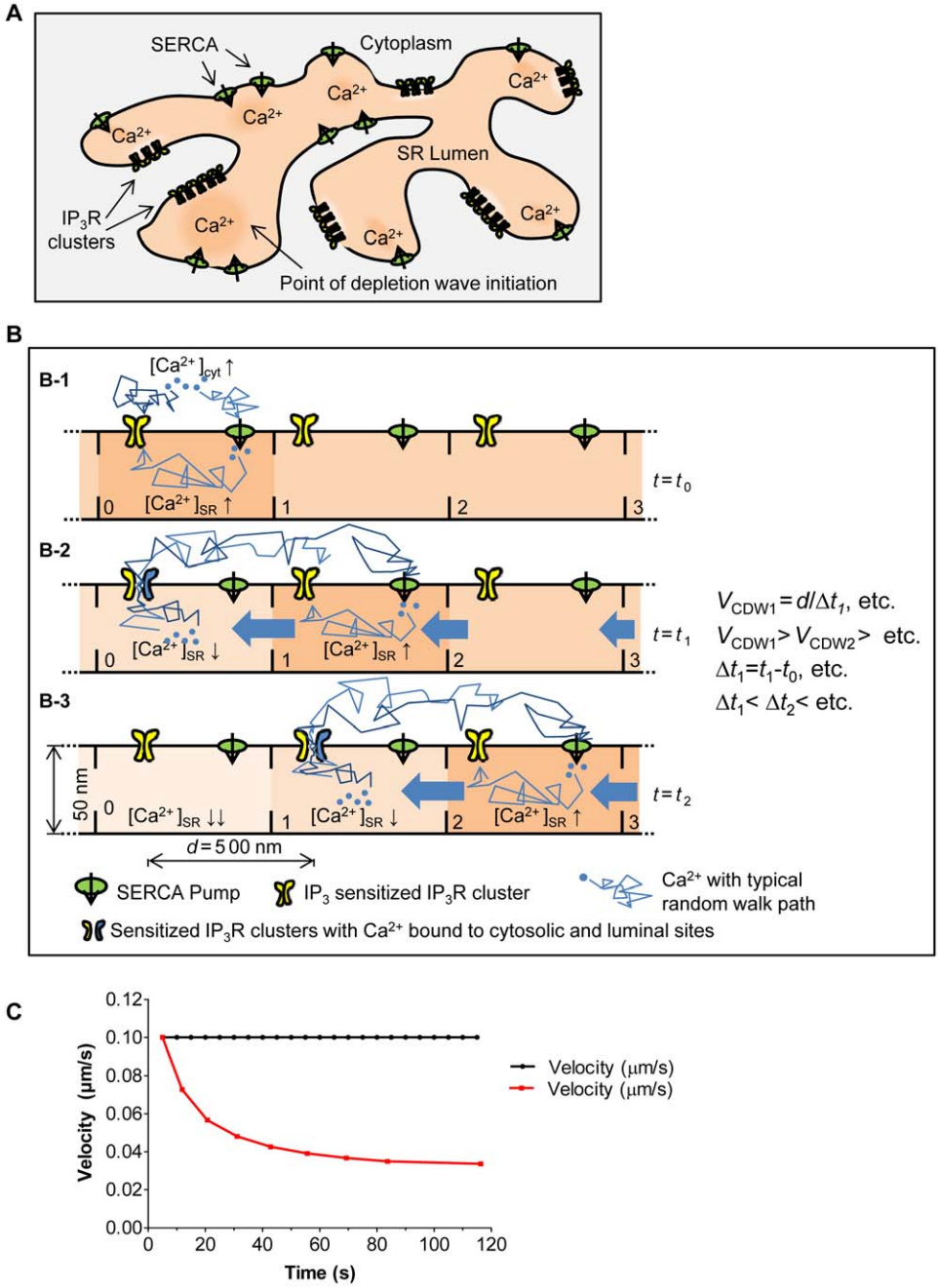

Figure 9. Simplified quantitative model for propagation of SR Ca^{2+} depletion waves. A) Schematic model of SR network depicting differential distribution of SR luminal Ca^{2+} sources (SERCA) and sinks (IP_3Rs). **B)** We represent a linear section of SR as a series of compartments (labelled 0, 1, 2, etc), between which Ca^{2+} transport is allowed. Panels B-1, B-2, & B-3 represent the same portion of model SR at three different times, t_0, t_1 and t_2. A wave initiating at compartment 0 in this model would move both left and right, but we focus only of the right-moving part for simplicity. Assuming that the $[IP_3]_{cyt}$ is such that the IP_3R is already Ca^{2+}-sensitized, a $[Ca^{2+}]_i$ fluctuation near the SR compartment 0 at $t = t_0$ raises the $[Ca^{2+}]_{SR}$ from a resting level to a threshold level, and thereby, causes the observed transient rise (B-1). This rise is followed by depletion of Ca^{2+} from compartment 0. Partial equilibration of luminal Ca^{2+} then takes place (blue block arrows between compartments), accompanied by an increase in $[Ca^{2+}]_{SR}$ in compartment 1 (B-2). Subsequently, $[Ca^{2+}]_{SR}$ in compartment 1 reaches a threshold value leading to the releases of (some of) its Ca^{2+}, which goes on to partially refill its nearest neighbouring locus (compartment 2), and so on (B-3). Ca^{2+} release from compartment 1 can trigger release from compartment 2, only after $[Ca^{2+}]_{SR}$ will have reached a critical level for Ca^{2+} release, which will take a time interval $\Delta t_2 = t_2 - t_1$. Due to the Ca^{2+} passage from compartment 2 to 1, Δt_2 must be greater than Δt_1, the interval it took to raise $[Ca^{2+}]_{SR}$ in 1 to the release level. Successive compartment refilling times to release level will get progressively longer because of the ability to re-equilibrate Ca^{2+} depletions. Assuming now that the CICR sustaining IP_3R clusters are on average equidistant at a length d (500 nm) from one another, the Ca^{2+} depletion wave velocity (v_{CDW}), as the wave reaches successive compartments, is given by V_{CDW1} $v_{CDW1} = d/\Delta t_1 > v_{CDW2} > \ldots > etc.$ Under the conditions of the reported experiments, disallowing Ca^{2+} communication between SR compartments in this model would translate in an equal interval Δt between the wave arrival at each compartment, and therefore in a constant wave velocity ($v_{CDW} = d/\Delta t$). **C)** Ca^{2+} depletion wave velocity *vs.* time calculated from our model, considering Ca^{2+} communicating (solid curve) or Ca^{2+} tight (dashed) SR compartments.
doi:10.1371/journal.pone.0055333.g009

Table 1. Symbols and data for the quantitative Model.

Quantity	Data	References
SR lumen cross-section	50 nm×50 nm	[46,47]
IP_3R cluster-cluster distance, *d*	500 nm	[46]
SR compartment volume	50 nm×50 nm×500 nm	[46,47,48]
SERCA refill rate	300 s^{-1}	[46]
Normal $[Ca^{2+}]_{SR}$, C_{SR}	500 μM	our observation
Critical $[Ca^{2+}]_{SR}$, C^*_{SR}	700 μM	our observation
Ca^{2+} shift from 1 to 0 (see Fig. 9B)	20%	our choice
Ca^{2+} shift from 2	5%	our choice
Ca^{2+} shift from 3	1%	our choice

doi:10.1371/journal.pone.0055333.t001

s. If we now assume that SR compartments 2, 3, etc lose part of their Ca^{2+} toward the depleted neighboring SR compartments by the percentages indicated in Table 1 (these values are arbitrarily chosen), their "normal" $[Ca^{2+}]_{SR}$ will be $C_{2,SR}$, $C_{3,SR}$, etc., where these values are *lower* than C_{SR}. The same line of reasoning then suggests that, for compartment 2 to release, its $[Ca^{2+}]_{SR}$ needs to change by $C^*_{SR} - C_{2,SR} > 200$ μM, which will take a time $\Delta t_2 > \Delta t_1$ and, in turn, yields a velocity for the second step as $v_{CDW,2} = d/\Delta t_2 < v_{CDW,1}$. To consider what would happen in a portion of SR with Ca^{2+} tight compartments, to a first degree of approximation, we can re-use the model above with 0% Ca^{2+} communication between compartments. It should be evident then that the interval needed to refill each compartment before release is the same as the putative wave progresses. Since the average inter-cluster distance is the same, the resulting wave velocity would be a constant value $v_{CDW} = d/\Delta t$ at each step. The results reported in Figure 9C were obtained by following this step-by-step procedure for about 100 seconds, which confirms that introduction of such luminal Ca^{2+} flux into the model indeed caused incremental decrease of the simulated Ca^{2+} depletion wave velocity (Fig. 9C, red trace).

Our proposed model clearly depends on populations of IP_3Rs and SERCA spread over the entire SR network. This appears to be the case for the SMCs used in this study as both SERCA (Fig. 10A) and IP_3Rs (Fig. 10B) display the same diffuse distribution as the D1SR and ER-Tracker.

Arrest of the ET-induced SR Depletion Wave at the Border of the Nuclear Envelope

Close inspection of the SR depletion waves also provides novel insight into sub-cellular differential Ca^{2+} signalling. Figure 11A presents snapshots of a depletion wave, which originates very close

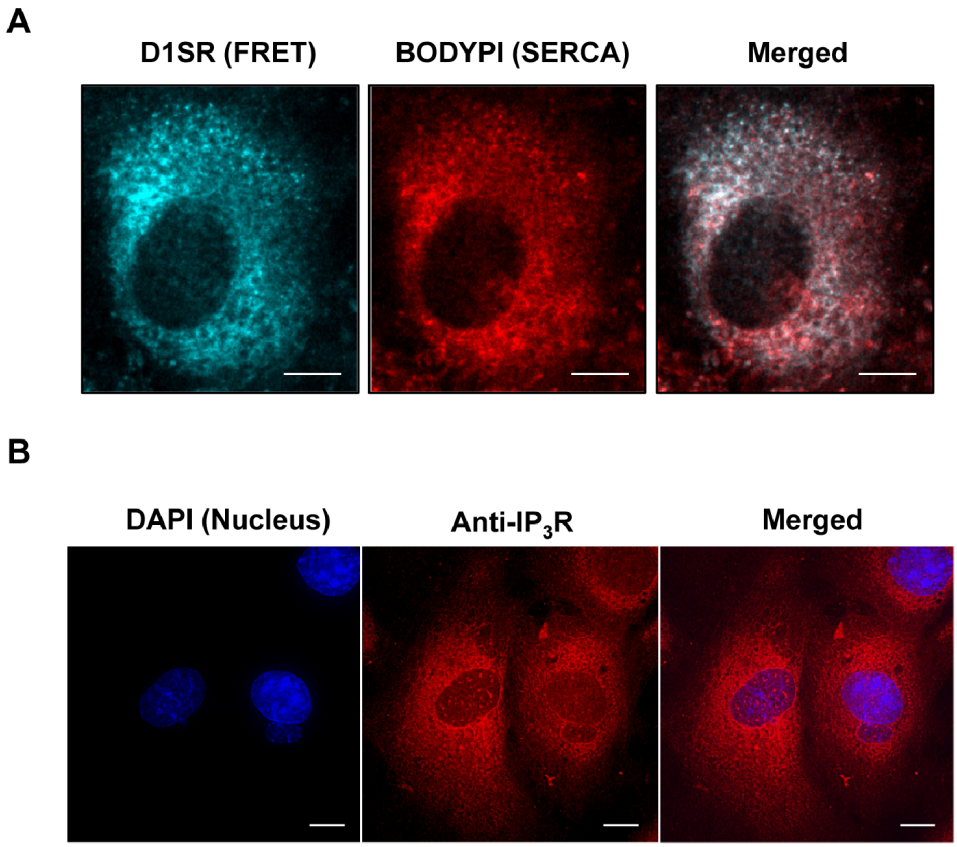

Figure 10. Distribution of SERCA and IP_3Rs in cultured rat aortic SMCs. A) Live snapshots of cultured rat aortic SMCs transfected with D1SR construct and treated with 1 μM of BODIPY® TR-X thapsigargin showing the distribution of SERCA in cultured SMCs. SERCA distribution follows the same pattern as SR luminal network as indicated by expression of D1SR indicator (FRET channel) within the SR lumen (scale bars, 10 μm). **B)** Receptors for IP_3 (IP_3Rs) were immuno-labelled using rabbit polyclonal antibody against IP_3R type I and Alexa-594 secondary antibody (Red). Images are representative of 29 cells imaged from four independent SMC cultures, and are shown as maximal intensity projections of de-convolved image stacks. Nucleus is labeled using DAPI (blue) (scale bars, 5 μm).
doi:10.1371/journal.pone.0055333.g010

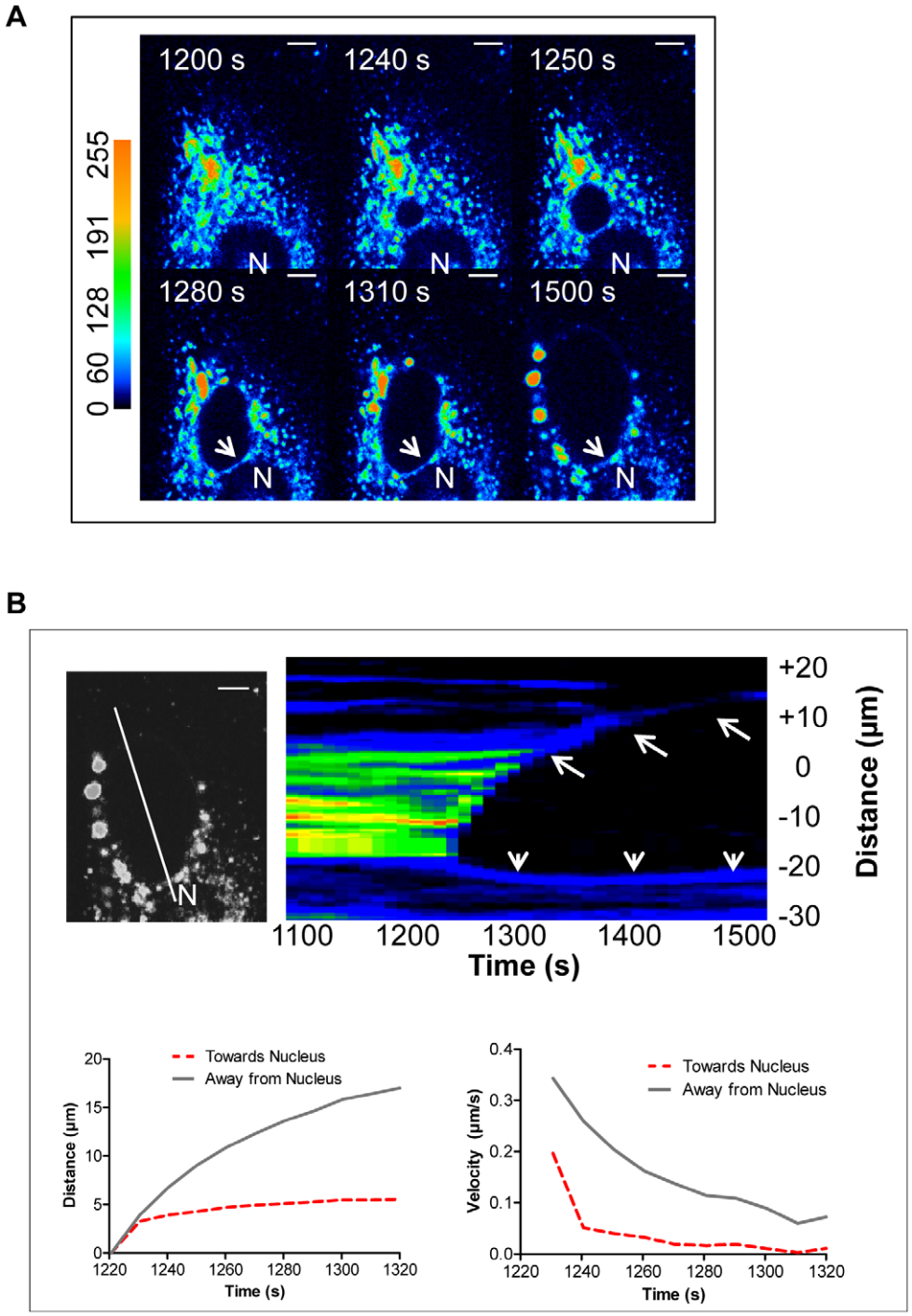

Figure 11. Arrest of the Ca^{2+} depletion waves at the border of the nuclear envelope. A) Snapshots (FRET channel) of SMCs treated with ET-1 (100 nM) in the absence of extracellular Ca^{2+}. The depletion wave is arrested at the nuclear envelope (white arrows) but progresses in the opposite upward direction (scale bars, 5 µm; N, nucleus). **B)** Line scan of Ca^{2+} signal through the point of origin of the depletion wave and heat map of the arrested wave. The depletion wave is unable to proceed through nuclear region and arrested at the nuclear border creating an almost straight line of Ca^{2+}-rich areas (white arrowheads), while progressing in the opposite direction (white arrows) (scale bars, 5 µm). Traces compare the distance travelled and velocity of the wave over time toward and away from the nuclear envelope from the point of origin.
doi:10.1371/journal.pone.0055333.g011

to the nucleus (see Movie S3). In this particular case, the shape of the wave front becomes oblong instead of circular, as it fails to involve the nuclear envelope (white arrows), and proceeds in the opposite peripheral direction. The asymmetry of this particular wave is clearly demonstrated by the heat map in Figure 11B. As shown, the distance traveled by the wave and its velocity drop dramatically when the wave collides with the nuclear envelope, without depleting its luminal Ca^{2+} content. In contrast, the pattern

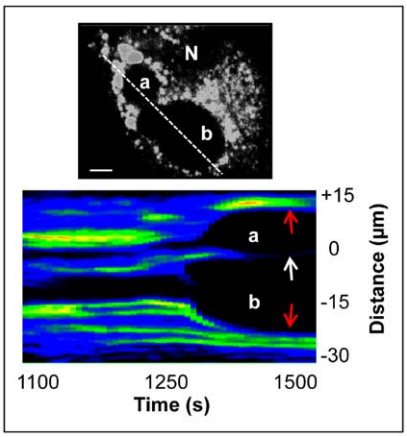

Figure 12. Colliding of neighbouring Ca^{2+} depletion waves. Line scan of Ca^{2+} signal through the point of origin of two neighbouring depletion waves (a & b) and the heat map of the colliding waves accentuate that the bright rim between two neighbouring waves disappears over time (white arrow), while the rims facing the plasma membrane persist (red arrows) (N, nucleus, scale bars, 5 μm).
doi:10.1371/journal.pone.0055333.g012

of two neighbouring SR depletion waves colliding with each other is clearly different from the case when a depletion wave encounters the nuclear envelope. As shown in Figure 12, in some cells, multiple Ca^{2+} depletion waves develop independently. In these cells, a line scan of the Ca^{2+} signal through the point of origin and through the border between neighbouring waves (a & b) shows that the depleted areas of colliding waves coalesce (white arrow) without a dividing line of Ca^{2+} loaded SR as seen at the periphery of both depletion waves (red arrows).

Discussion

In this first report of Ca^{2+} depletion waves in the smooth muscle sarcoplasmic reticulum, we describe a crucial role for luminal $[Ca^{2+}]_{SR}$ in the initiation and propagation of cytoplasmic Ca^{2+} waves. This additional insight was gained because the dynamics of SR Ca^{2+} depletion do not simply mirror $[Ca^{2+}]_i$ elevations, but display their own unique characteristics. The disparity between the $[Ca^{2+}]_i$ and $[Ca^{2+}]_{SR}$ transients is most likely due to significant contributions by plasma membrane Ca^{2+} fluxes to smooth muscle Ca^{2+} homeostasis and excitation.

Iino's hypothesis that Ca^{2+} waves in VSM are propagated by regenerative CICR at the IP_3Rs [4] was recently corroborated by a well-controlled study by McCarron and collaborators on freshly isolated SMCs, voltage clamped and incubated in a Ca^{2+} free medium [22]. Progression of the wave front by CICR requires that the released Ca^{2+} raises the local $[Ca^{2+}]_i$ in the neighbouring nano-domain occupied by IP_3Rs, which are about to be activated. Although such spatio-temporal resolution of cytoplasmic Ca^{2+} waves has not yet been reported, our data conclusively show that this is indeed the case. The only possible explanation for the increased $[Ca^{2+}]_{SR}$ at the wave rim is that the SERCA pumps respond to the local $[Ca^{2+}]_i$ elevations before activation of IP_3R ahead of the Ca^{2+} wave. Our observation of a diffuse distribution of both SERCA and IP_3R over the entire SR (see Fig. 10) corroborates this view. Moreover, our conclusions show Ca^{2+} diffuses from an elevated $[Ca^{2+}]_i$ site, to a neighbouring site containing an IP_3R cluster more rapidly than the propagation of a depletion wave. This supports the mechanism of a wave of CICR, and is experimentally confirmed by the increased $[Ca^{2+}]_{SR}$ at the wave rim due to SERCA-mediated Ca^{2+} uptake in response to the local $[Ca^{2+}]_i$ elevation before activation of IP_3Rs, ahead of the Ca^{2+} wave.

The transient elevations of $[Ca^{2+}]_{SR}$ at the site of wave initiation and at the wave front, directly demonstrate local interactions between adjacent SR sites, which depend on SR luminal continuity and in principle could be readily influenced by other Ca^{2+} transporting organelles, such as mitochondria and lysosomes in shaping the smooth muscle Ca^{2+} signal [30,31,32,33,34]. It is evident that the elevated $[Ca^{2+}]_{SR}$ at the origin and at the rim of the wave plays a crucial role in wave initiation and propagation, underscoring the importance of previous reports demonstrating that $[Ca^{2+}]_{SR}$ has a stimulatory role in IP_3R-mediated Ca^{2+} release [35,36,37].

In fact, several reports make a strong case for the existence of a luminal excitatory Ca^{2+}-binding site on IP_3R, which would provide a straightforward explanation for the stimulating effects of $[Ca^{2+}]_{SR}$ [27,28,38,39]. Regulation of IP_3R by luminal Ca^{2+} suggests a mechanism for Ca^{2+} wave initiation based on local $[Ca^{2+}]_{SR}$ fluctuations caused by random opening of IP_3Rs and separation of Ca^{2+} sources (SERCA) and sinks (IP_3Rs) in the walls of the SR lumen (see Fig. 9). It is conceivable that the "Frequent Discharge Sites" observed by Bolton and coworkers [40] were due to specific local ultra-structural characteristics of the SR which favour focal $[Ca^{2+}]_{SR}$ fluctuations. One of these is closeness to the nucleus, which has been shown in HeLa cells to delay the decay of IP_3R-generated Ca^{2+} puffs, due to decreased sequestering/buffering [25,26].

A relevant question is why these waves were observed only in the absence of external Ca^{2+}. One plausible answer is that removal of external Ca^{2+} causes marked lowering of $[Ca^{2+}]_i$ and thereby delays SR Ca^{2+} release stimulated by ET-1. In our VSMC preparation, we have shown that the release is mediated by opening of IP_3Rs (see Fig. 7). It is likely that the reduced $[Ca^{2+}]_i$ due to removal of external Ca^{2+} lowers the rate of IP_3 synthesis by phospholypase C, and thus increases the time required for IP_3 concentration to reach a threshold value [41,42]. The latency period would be further increased because the low $[Ca^{2+}]_i$ would also raise the threshold for IP_3-mediated activation. The consequently slower rates of spontaneous discharge combined with the lack of SR refilling would greatly enhance the development of Ca^{2+} depletion waves. On the other hand, in the presence of extracellular Ca^{2+}, rapid SR refilling could obscure the depletion process. In addition, activation of clusters of IP_3Rs at much higher frequency would prevent the development of full Ca^{2+} depletion waves. Since it was essential to separate trans-plasma membrane fluxes from the Ca^{2+} release process, we simply removed the extracellular Ca^{2+} component, a procedure which we and numerous previous studies have shown to not have deleterious effects on the SR [16,20,43,44,45]. Thus, we conclude that the observed Ca^{2+} depletion waves provide valuable new insight into a regulatory role of $[Ca^{2+}]_{SR}$ in the processes of Ca^{2+} wave initiation and propagation.

Finally, the arrest of the SR depletion wave at the border of the nuclear envelope indicates that, as has been shown previously [17], the two membrane systems may differ with respect to their respective Ca^{2+} transport mechanisms. Figure 10B strongly suggests that the nuclear envelope does contain IP_3R, but whether these are located in the membrane facing the cytoplasm or the inner membrane facing the nucleoplasm is an open question. Nevertheless, the observation that the wave does not deplete the nuclear envelope, could be of physiological importance in terms of

segregation of dynamic Ca^{2+} signalling of vasoconstriction from functions such as gene transcription.

In conclusion, the findings presented in this study provide new insight into the mechanisms whereby the ER/SR, the main Ca^{2+} regulatory organelle in living cells, determines spatial and temporal characteristics of cellular Ca^{2+} signalling, which differentially control cellular migration, growth, proliferation and apoptosis in health and disease.

Supporting Information

Movie S1 3-D structure of rat SMCs transfected with D1SR.
(WMV)

Movie S2 ET-induced SR calcium depletion wave.
(WMV)

Movie S3 Arrest of depletion wave at the nuclear envelope.
(WMV)

Acknowledgments

We thank Dr. Wayne Chen at Libin Cardiovascular Institute of Alberta, University of Alberta for providing the D1SR construct and helpful discussions. We also thank Dr. Kevin Hodgson at UBC Bioimaging Facility, and Dr. Jingson Wang at the Child & Family Research Institute Imaging Core, for their technical assistance with the confocal imaging.

Author Contributions

Conceived and designed the experiments: ME CvB. Performed the experiments: ME YYHC AYT. Analyzed the data: YYHC AYT JGH NF. Contributed reagents/materials/analysis tools: NF. Wrote the paper: ME NF CvB.

References

1. Nicotera P, Orrenius S (1998) The role of calcium in apoptosis. Cell Calcium 23: 173–180.
2. Kumar B, Dreja K, Shah SS, Cheong A, Xu SZ, et al. (2006) Upregulated TRPC1 channel in vascular injury in vivo and its role in human neointimal hyperplasia. Circ Res 98: 557–563.
3. van Breemen C, Poburko D, Okon EB (2006) TRP proteins: a new dimension in the treatment of occlusive vascular disease. Circ Res 98: 446–447.
4. Iino M, Kasai H, Yamazawa T (1994) Visualization of neural control of intracellular Ca2+ concentration in single vascular smooth muscle cells in situ. EMBO J 13: 5026–5031.
5. Aalkjaer C, Nilsson H (2005) Vasomotion: cellular background for the oscillator and for the synchronization of smooth muscle cells. Br J Pharmacol 144: 605–616.
6. Berridge MJ, Lipp P, Bootman MD (2000) The versatility and universality of calcium signalling. Nat Rev Mol Cell Biol 1: 11–21.
7. Carafoli E, Santella L, Branca D, Brini M (2001) Generation, control, and processing of cellular calcium signals. Crit Rev Biochem Mol Biol 36: 107–260.
8. Iino M (2010) Spatiotemporal dynamics of Ca2+ signaling and its physiological roles. Proc Jpn Acad Ser B Phys Biol Sci 86: 244–256.
9. Berridge MJ (1994) The biology and medicine of calcium signalling. Mol Cell Endocrinol 98: 119–124.
10. Dai JM, Syyong H, Navarro-Dorado J, Redondo S, Alonso M, et al. (2010) A comparative study of alpha-adrenergic receptor mediated Ca(2+) signals and contraction in intact human and mouse vascular smooth muscle. Eur J Pharmacol 629: 82–88.
11. Neylon CB, Hoyland J, Mason WT, Irvine RF (1990) Spatial dynamics of intracellular calcium in agonist-stimulated vascular smooth muscle cells. Am J Physiol 259: C675–686.
12. Iino M (1987) Calcium dependent inositol trisphosphate-induced calcium release in the guinea-pig taenia caeci. Biochem Biophys Res Commun 142: 47–52.
13. Lo Russo A, Passaquin AC, Andre P, Skutella M, Ruegg UT (1996) Effect of cyclosporin A and analogues on cytosolic calcium and vasoconstriction: possible lack of relationship to immunosuppressive activity. Br J Pharmacol 118: 885–892.
14. Palmer AE, Giacomello M, Kortemme T, Hires SA, Lev-Ram V, et al. (2006) Ca2+ indicators based on computationally redesigned calmodulin-peptide pairs. Chem Biol 13: 521–530.
15. Palmer AE, Tsien RY (2006) Measuring calcium signaling using genetically targetable fluorescent indicators. Nat Protoc 1: 1057–1065.
16. Poburko D, Liao CH, van Breemen C, Demaurex N (2009) Mitochondrial regulation of sarcoplasmic reticulum Ca2+ content in vascular smooth muscle cells. Circ Res 104: 104–112.
17. Wu G, Xie X, Lu ZH, Ledeen RW (2009) Sodium-calcium exchanger complexed with GM1 ganglioside in nuclear membrane transfers calcium from nucleoplasm to endoplasmic reticulum. Proc Natl Acad Sci U S A 106: 10829–10834.
18. Lee CH, Poburko D, Kuo KH, Seow C, van Breemen C (2002) Relationship between the sarcoplasmic reticulum and the plasma membrane. Novartis Found Symp 246: 26–41; discussion 41–27, 48–51.
19. Leijten PA, van Breemen C (1986) The relationship between noradrenaline-induced contraction and 45Ca efflux stimulation in rabbit mesenteric artery. Br J Pharmacol 89: 739–747.
20. McCarron JG, Chalmers S, Muir TC (2008) "Quantal" Ca2+ release at the cytoplasmic aspect of the Ins(1,4,5)P3R channel in smooth muscle. J Cell Sci 121: 86–98.
21. Vallot O, Combettes L, Jourdon P, Inamo J, Marty I, et al. (2000) Intracellular Ca(2+) handling in vascular smooth muscle cells is affected by proliferation. Arterioscler Thromb Vasc Biol 20: 1225–1235.
22. McCarron JG, Chalmers S, MacMillan D, Olson ML (2010) Agonist-evoked Ca(2+) wave progression requires Ca(2+) and IP(3). J Cell Physiol 224: 334–344.
23. Lee CH, Rahimian R, Szado T, Sandhu J, Poburko D, et al. (2002) Sequential opening of IP(3)-sensitive Ca(2+) channels and SOC during alpha-adrenergic activation of rabbit vena cava. Am J Physiol Heart Circ Physiol 282: H1768–1777.
24. Berridge MJ (1991) Cytoplasmic calcium oscillations: a two pool model. Cell Calcium 12: 63–72.
25. Thomas D, Lipp P, Berridge MJ, Bootman MD (1998) Hormone-evoked elementary Ca2+ signals are not stereotypic, but reflect activation of different size channel clusters and variable recruitment of channels within a cluster. J Biol Chem 273: 27130–27136.
26. Swillens S, Champeil P, Combettes L, Dupont G (1998) Stochastic simulation of a single inositol 1,4,5-trisphosphate-sensitive Ca2+ channel reveals repetitive openings during 'blip-like' Ca2+ transients. Cell Calcium 23: 291–302.
27. Sienaert I, De Smedt H, Parys JB, Missiaen L, Vanlingen S, et al. (1996) Characterization of a cytosolic and a luminal Ca2+ binding site in the type I inositol 1,4,5-trisphosphate receptor. J Biol Chem 271: 27005–27012.
28. Missiaen L, De Smedt H, Parys JB, Sienaert I, Vanlingen S, et al. (1996) Effects of luminal Ca2+ on inositol trisphosphate-induced Ca2+ release: facts or artifacts? Cell Calcium 19: 91–93.
29. Rainbow RD, Macmillan D, McCarron JG (2009) The sarcoplasmic reticulum Ca2+ store arrangement in vascular smooth muscle. Cell Calcium 46: 313–322.
30. Rizzuto R, Bernardi P, Pozzan T (2000) Mitochondria as all-round players of the calcium game. J Physiol 529 Pt 1: 37–47.
31. Rizzuto R, Duchen MR, Pozzan T (2004) Flirting in little space: the ER/mitochondria Ca2+ liaison. Sci STKE 2004: re1.
32. Pizzo P, Pozzan T (2007) Mitochondria-endoplasmic reticulum choreography: structure and signaling dynamics. Trends Cell Biol 17: 511–517.
33. Zhang F, Xia M, Li PL (2010) Lysosome-dependent Ca(2+) release response to Fas activation in coronary arterial myocytes through NAADP: evidence from CD38 gene knockouts. Am J Physiol Cell Physiol 298: C1209–1216.
34. Kinnear NP, Wyatt CN, Clark JH, Calcraft PJ, Fleischer S, et al. (2008) Lysosomes co-localize with ryanodine receptor subtype 3 to form a trigger zone for calcium signalling by NAADP in rat pulmonary arterial smooth muscle. Cell Calcium 44: 190–201.
35. Missiaen L, Taylor CW, Berridge MJ (1992) Luminal Ca2+ promoting spontaneous Ca2+ release from inositol trisphosphate-sensitive stores in rat hepatocytes. J Physiol 455: 623–640.
36. Missiaen L, De Smedt H, Droogmans G, Casteels R (1992) Ca2+ release induced by inositol 1,4,5-trisphosphate is a steady-state phenomenon controlled by luminal Ca2+ in permeabilized cells. Nature 357: 599–602.
37. Shmygol A, Wray S (2005) Modulation of agonist-induced Ca2+ release by SR Ca2+ load: direct SR and cytosolic Ca2+ measurements in rat uterine myocytes. Cell Calcium 37: 215–223.
38. Missiaen L, Taylor CW, Berridge MJ (1991) Spontaneous calcium release from inositol trisphosphate-sensitive calcium stores. Nature 352: 241–244.
39. Taylor CW, Tovey SC (2010) IP(3) receptors: toward understanding their activation. Cold Spring Harb Perspect Biol 2: a004010.
40. Gordienko DV, Greenwood IA, Bolton TB (2001) Direct visualization of sarcoplasmic reticulum regions discharging Ca(2+) sparks in vascular myocytes. Cell Calcium 29: 13–28.
41. Meyer T, Stryer L (1988) Molecular model for receptor-stimulated calcium spiking. Proc Natl Acad Sci U S A 85: 5051–5055.
42. Meyer T, Stryer L (1991) Calcium spiking. Annu Rev Biophys Biophys Chem 20: 153–174.
43. Rizzuto R, Brini M, Murgia M, Pozzan T (1993) Microdomains with high Ca2+ close to IP3-sensitive channels that are sensed by neighboring mitochondria. Science 262: 744–747.

44. Syyong HT, Yang HH, Trinh G, Cheung C, Kuo KH, et al. (2009) Mechanism of asynchronous Ca(2+) waves underlying agonist-induced contraction in the rat basilar artery. Br J Pharmacol 156: 587–600.
45. Takeda Y, Nystoriak MA, Nieves-Cintron M, Santana LF, Navedo MF (2011) Relationship between Ca2+ sparklets and sarcoplasmic reticulum Ca2+ load and release in rat cerebral arterial smooth muscle. Am J Physiol Heart Circ Physiol 301: H2285–2294.
46. Lee CH, Poburko D, Kuo KH, Seow CY, van Breemen C (2002) Ca(2+) oscillations, gradients, and homeostasis in vascular smooth muscle. Am J Physiol Heart Circ Physiol 282: H1571–1583.
47. Poburko D, Kuo KH, Dai J, Lee CH, van Breemen C (2004) Organellar junctions promote targeted Ca2+ signaling in smooth muscle: why two membranes are better than one. Trends Pharmacol Sci 25: 8–15.
48. Foskett JK, White C, Cheung KH, Mak DO (2007) Inositol trisphosphate receptor Ca2+ release channels. Physiol Rev 87: 593–658.